FATIGUE LIFE PREDICTION OF A CRANE GIRDER: COMPARING HOT SPOT STRESS AND FRACTURE MECHANICS APPROACHES

K. Hectors[1,2], W. De Waele[2]

Ageing infrastructure is a major concern for industries across Europe. In this paper an overhead crane girder that is part of an ageing fleet of nearly identical structures with known fatigue cracking problems is studied. A global finite element model is developed, validated and used to drive submodels of different scales. Using load spectra based on real operational data, hot spot stress and fracture mechanics based fatigue lifetime calculations are performed using in-house developed numerical frameworks. Supported by a thorough literature review, the results of both methods are critically analyzed and compared. The estimated lifetime obtained using a fracture mechanics approach and an initial crack of only 0.1mm deep, differs two orders of magnitude compared to the endurance based hot spot stress approach. The study also revealed that a fracture mechanics based assessment is overly sensitive to the initial crack dimensions and material properties. Finally it is shown that the often used assumption of a constant aspect ratio can lead to overly conservative results.

INTRODUCTION

Crane runway girders support the overhead cranes (an example is shown in figure 1) used in manufacturing and production halls in heavy industry such as steel production plants. Crane runway girders are steel structures that span large sections and are subjected to a wide range of multi-axial, variable amplitude loading conditions which makes them especially prone to fatigue. Furthermore, many girders that were built in the early 1970's have flange gusset details which, although not used anymore, have poor fatigue strength (Tominaga et al. [1]). Milman [2] indicated that crane girders built in the early 1970's mostly suffer from cracking of the fillet welds that connect the flanges to the web, the stiffeners to the web and the connections between flanges. Numerous articles on fatigue cracks occurring in crane runway girders have been published, examples are the works of Patrikeev [3], Kuwamura and Hanzawa [4], Demo and Fisher [5]. More recently, Wardenier et al. [6] reported cracks that initiated in the top flange at the weld toe of the full penetration weld that connects the top flange to the web. Ávila et al. [7] report cracks occurring in cover plates welded to the bottom flange of the main girder as well as cracks occurring in connecting plates between the main girder and the lateral support structure. An overview of the most common crack locations is shown in figure 2. A number of studies have been published on numerical fatigue life assessment of operational crane runway girders. This will be discussed in more detail in the next section.

[1] SIM vzw, Tech Lane Ghent Science, Park / Campus A 48, BE-9052, Zwijnaarde, Belgium.
[2] Ghent University, Faculty of Engineering and Architecture, Department EMSME, Laboratory Soete, Technologiepark 46, BE-9052 Zwijnaarde, Belgium

Cagalyan et al. [8] instrumented a girder with strain gauges to validate a finite element model and used former operational records to define a fatigue spectrum. They performed a fatigue assessment of different crane girders and details in accordance with the Standard specifications for highway bridges (AASHTO 1998 [9]). Tong et al. [10] studied the fatigue strength of a series of end-coped crane runway girders after fatigue cracks were observed. A finite element model of the girders was developed and validated using strain gauge measurements. Based on 1/5 scale models and the validated finite element models, Tong et al. proposed a design guide for end-coped crane runway girders. They also concluded that the AASHTO specifications are not sufficient for designing these end-coped details. The design of these details is based on the nominal stress approach and the detail categories corresponding to the studied details were found to be non-conservative. Pelayo et al. [11] performed a study on a cracked runway girder and similar conclusions were drawn with respect to the former Spanish UNE 76202:1992 standard and Eurocode EN-1993-1-9. They concluded that fatigue life estimations based on the design spectra provided in both standards are unreliable and can be significantly improved if an operational stress spectrum is used. Wardenier et al. [12] found that fatigue classes in EN 1993-1-9 and EN 1993-1-3 are overly conservative for crane runway girders with multi-layered full penetration welds loaded in compression. Their conclusion is based on an experimental study of ½ scaled equivalent welded I-sections. Other fatigue studies of crane runway girders based on the endurance approach have been performed by Kossakowski et al. [13], Citarelli and Feldmann [14], Vašková et al. [15].

Although the nominal stress based endurance approach is useful in the design stage, it does not explicitly take local stress raising effects, e.g. the presence of welds, into account. Also, many structural details cannot be unambiguously classified in the predefined fatigue classes of, for example, Eurocode. The hot spot stress approach provides a significant improvement over the nominal stress approach as it accounts for the structural geometry of the joint. It also allows for a more straightforward selection of an S-N curve compared to the nominal stress approach where the assessed joint is not always explicitly categorized in one of the detail categories. Since fatigue cracks observed in crane runway girders mostly initiate at the weld toes [12], the hot-spot stress method described in the IIW-2259-15 guidelines (Hobbacher [16]) can be used to perform a more accurate fatigue assessment of welded structural details (Niemi et al. [17]). Although extensively used for other civil structures such as bridges (e.g. Akhlaghi [18], Chan et al. [19], Ding et al. [20]); application to crane runway girders in literature is very limited (e.g. Hectors et al. [21]).

The most comprehensive manner to assess the remaining useful lifetime of a cracked structural detail is the use of linear-elastic fracture mechanics (LEFM). Ávila et al. [7] used the FRANC2D finite element software to determine mode I stress intensity factors (SIF) K_I for a propagating crack in a crane runway. The K_I values were used to determine the fatigue life up to a critical crack dimension. In the work of Ávila et al., the K_I calculation is based on a simplified 2D model (only the crack depth is taken into account) and the specifics of the model (boundary conditions, applied loads, …) are not clearly mentioned. Significant advancements have been made by Rettenmeier et al. [22], [23]. They studied the initiation and propagation of cracks starting at the root of fillet welds between the crane rail and top flange of the girder due to rolling contact fatigue. The studied weld is subjected to highly non-proportional mixed mode crack tip loading. In order to account for this, global deformations were determined using a crack free global model and then applied as boundary

conditions to a cracked 3D submodel. The crack tip stress state below the rail was found to be mode II dominated with significant mode III presence, whilst K_I was found to be negligible. Because of the shear mode II dominance, Rettenmeier et al. [23] used the cyclic shear stress intensity factor ΔK_τ to determine the propagation stage fatigue life. The crack propagations simulations were started from an initial crack depth $a_0 = 1$ mm to final through-thickness crack of $a \approx 7.5$ mm. By transferring the global model results to the submodel, the conditions that govern the crack tip stress state are much more accurately represented than in the method used by Ávila et al. [7]. Furthermore, the use of a 3D geometry makes it possible to explicitly account for the elliptical crack geometry. Some simplifications and disadvantages can however be identified. The authors assumed that the aspect ratio of the initial elliptical crack $a/c = 1/3$ remains constant and therefore the SIF was only determined at the deepest point of the crack. Furthermore, the use of a conventional finite element analysis for the determination of the SIFs requires an extremely fine and well defined mesh since the mesh needs to conform to the crack shape. As the crack propagates, it is also required to continuously remesh the model. This is computationally expensive and not very robust for more complex models.

Based on the available literature discussed in the preceding paragraph it is clear that fatigue design of crane runway girders is conventionally based on endurance based fatigue calculations. Although some research is available on the application of more advanced fracture mechanics based methods for fatigue assessment of crane girders, its application remains very limited. In this paper, a multi-dimensional modelling approach is combined with both the hot spot stress (HSS) based endurance method and an XFEM based fracture mechanics method to assess a structural detail of an operational crane runway girder. The development and details of the endurance based numerical framework have been reported in Hectors et al. [21], [24]. An industrial crane runway girder has been instrumented with optical fibre Bragg sensors and the fibre optic strain measurements are used to validate a global finite element model. A submodel for which the boundary conditions are governed by the global model is used for both the hot spot stress and the fracture mechanics based analyses. To overcome shortcomings of the conventional finite element method for crack propagation analysis, an in-house developed framework for XFEM based crack propagation simulations is used.

NUMERICAL METHODS

In this study a comparison will be made between a hot-spot stress approach for fatigue lifetime estimation and an XFEM-based fatigue crack propagation analysis. The hot spot stresses are determined using an in-house developed framework for fully automated calculation of hot spot stresses and fatigue life; reference is made to [24] for a full description. Fatigue life of the selected joint detail for a variable load spectrum is determined using Miner's linear damage accumulation rule; failure is assumed when the damage parameter $D = 1$. Hot spot stresses are calculated based on the maximum principal stresses at $0.4t$ and $1.0t$ in front of the weld toe as recommend in IIW-2259-15 [16]. The FAT90 S-N curve as detailed in IIW-2259-15 is used to assess the structural detail. This S-N curve is bilinear, following the knee-point at 10^7 cycles it continues with a reduced slope.

The XFEM based fatigue crack propagation analyses are also done using in-house developed code. Obviously, the fatigue life of a structural component can be split in two stages, crack initiation and crack propagation. Crack propagation makes up the largest portion of service life of welded joints and it is therefore possible to use fracture mechanics for fatigue life estimations [16]. The fatigue life calculated using a fracture mechanics approach is defined as the number of cycles it takes

for an initial crack with depth a_0 to reach a final crack depth a_f. Determination of the crack propagation rate da/dN is, in its simplest form, a relation between the stress intensity factor range ΔK and the material parameters known as the Paris law:

$$\frac{da}{dN} = C\Delta K^m \quad (1)$$

Here C and m are material dependent properties. Since the material properties of the actual structure are not known, the recommended material properties for austenitic steels in air were adopted from BS7910:2019 [25], they are reported in $0.67t$ and t.

table 1. For the fracture mechanics parameters the 'mean + 2 standard deviations' law for fatigue ratio $R \geq 0.5$ is used as recommended by the same standard to assess welded components. The Abaqus 2020 XFEM solver is used to determine the mode I stress intensity factors along the crack front for a unit load case. Using these data as input, an independent Python code is used to calculate the stress intensity factor range ΔK_I along the crack front based on the defined load spectrum. The Paris law is then used to determine the crack growth rate da/dN and the corresponding number of cycles required to propagate the crack over a predetermined increment. Finally, the crack geometry of the XFEM model is updated accordingly and a new stress intensity factor solution is determined. The crack front geometry is not assumed to adhere to a constant aspect ratio as is the case in many studies, but is updated based on the local K_I solutions.

Both the assumed initial and final crack depth will have a strong influence on the final fatigue lifetime estimation. A number of recommendations exist for the initial crack size with sizes ranging from 0.01 to 3 mm (e.g. Rettenmeier et al. [23], Hobbacher [16] and Radaj et al. [26]). Radenkovic [27] used a_0 values ranging from 0.01 mm to 0.03 mm. Bokalrud and Karlson [28] found a_0 to be exponentially distributed with mean crack size of 0.11 mm for actual welded details in ship hull structures. This distribution was also adopted by Ayala-Uraga and Moan [29] in a study to evaluate weld fatigue sensitivity to the initial crack depth. Moan et al. [30] found an exponential distribution of a_0 with a mean of 0.19 mm in a study on the initial sizes of cracks detected in tubular joints of a jacket located in the North Sea. Others refer to the work of Gurney [31] who used $a_0 = 0.15$ mm and an aspect ratio of $a{:}\,c = 0.2$ (2c corresponds to the width of a semi-elliptical crack). Schumacher et al. [32] used $a_0 = 0.2$ mm and $a_0 = 0.4$ mm, and Lotsberg [33] who used $a{:}\,c = 0.2$ and a_0 = 0.03 mm. Darcis et al. [34] found that an initial crack depth in the range between 0.005 mm and 0.03 mm with a mean value 0.015 mm yield fatigue live estimations comparable to the FAT71 S-N curve of Eurocode 3 for stress ranges above the endurance limit.

Since the recommendations of the IIW are used in this study for the hot spot stress approach, their recommendation of an initial depth a_0 = 0.1 mm for a crack starting at a weld toe has been used. This value can be considered as conservative in comparison to the above reported mean initial crack sizes found in actual structures. The final crack length is typically defined as a fraction of the plate thickness and mainly depends on the expected failure mode. Common values for the final crack length range between $0.5t$ and t with t the plate or wall thickness (i.e. a through-thickness crack) [26]. In this work the effect of the final crack length is studied by comparing fatigue lives for $a_f = 0.5t, 0.67t$ and t.

TABLE 1: Material properties

E	ν	ΔK_{th} $[MPa\sqrt{m}]$	C	m
$200\ GPa$	0.3	2	$9.38 \cdot 10^{-10}$	5.1

It has been pointed out in literature that use of coupled fracture modes and calculation of an effective stress intensity factor should be considered in the case of multi-axial stress conditions (e.g. Qian and Fatemi [35]). In this work K_{II} and K_{III} are neglected as preliminary results showed that they have a rather limited effect on the crack growth rate in the studied model. Thus planar crack growth is assumed in this work and the effective stress intensity factor range $\Delta K_{eff} = \Delta K_1$.

Description of the global model and its validation

The structure studied in this paper is an overhead crane runway girder with a longitudinal span of 20m. It comprises a main girder that is reinforced with a lattice structure. The girder has to support two cranes that traverse the production hall. The cranes have a transverse span of 32m and a total (unloaded) mass of 102.5 and 135.5 metric tonnes, respectively. The cranes are used to transport steel coils with masses up to 35 metrics tonnes. The structure has been constructed from S355 steel. The actual material properties of both steel and weld metal are however unknown; documentation on material properties and welding procedures was not preserved. An elastic modulus of 200 GPa and a Poisson coefficient of 0.3 are used for the finite element models.

A global finite element of the overhead crane girder has been developed in the finite element software Abaqus 2020 and is used to simulate its deformations and the corresponding nominal stresses for different load cases. The different joint details are not modeled explicitly, but the main structural elements and boundary conditions are. Figure 3 shows a 3D model of the crane girder with indication of its principal features. The most important section is the main supporting girder (a) as it bears the majority of the load. Approximately every two meters, transversal T-profile stiffeners (b) have been welded to both sides of the web to prevent buckling. The stiffeners are also welded to the lower side of the top flange but do not extend to the bottom flange. The lattice structure (c) attached to the main girder was modelled using quadratic beam elements; its main function is to divert the loads away from the main girder. On top of the supporting lattice structure lies a walkway (d) that has been welded to it. This walkway was also included in the model as it increases the transverse stiffness of the structure considerably. The main girder, the walkway and the web stiffeners were modelled using 8-node doubly curved thick shell elements with reduced integration.

In the scope of the Flemish ‘SafeLife’ project, the studied overhead girder has been fitted with 56 optical fibre Bragg grating (FBG) sensors distributed over four lines (two on the top and two on the bottom flange) to measure the strains in the main girder during operation. Two temperature sensors were installed to filter out strain variations due to ambient temperature changes. Figure 4 shows an overview of the sensors locations.

To validate the global element model, a quasi-static reference ‘event’ was performed during which strains were measured. An empty crane was moved to the mid-section of the girder, a coil of approximately 35 metric tonnes was then lifted and placed down again. Figure 5 shows the measured

strains compared to the strains obtained using the finite element model. The outer measurement points in the experimental data correspond to the strains measured by the sensors on the neighboring girders, the girders represented as opaque in figure 4.

Figure 5 shows that a very good agreement was found between the experimental measurements and the results of the finite element model. The two peaks that are visible in the strain trace of the compression zone correspond to the locations where the wheel loads have been applied to the finite element model, causing a singularity. It can be seen that both the finite element model and the experimental results show an (albeit expected) increased stress where the cover plate is welded to the bottom flange ends. This corresponds to the detail that is also explicitly shown in figure 4.

Description of the submodel

The relatively high nominal stress combined with the stress raising effect of the local geometry, make the end of the welded bottom flange cover plate a fatigue critical detail as was confirmed by both the numerical and experimental results. Moreover, fatigue cracks in similar details have already been observed in other crane girders. Two examples are shown in figure 6**.** For these reasons the cover plate end has been selected as the detail of interest for this study. A detailed representation of the structural detail is constructed using a fully 3D solid mesh. Figure 7 shows an overlay of the submodel and the global model. By changing the modelling space from shell to solid and increasing the mesh density significantly, a more representative and accurate result can be obtained. The boundary conditions of the submodel are governed by the global model. A nodal-based submodelling technique is used, where the displacements of the nodes in the global model are transferred to the boundary nodes of the submodel.

To accurately perform the crack growth analysis, a submodel of the submodel (further called sub-submodel) had to be developed. The reason being that the crack with a starting depth of 0.1 mm and a final crack depth of 29 mm (corresponding to a through-thickness crack) differ an order of magnitude and thus the required mesh density and submodel size differ significantly between the start and end of the fatigue crack propagation simulation. In order to achieve manageable calculation times, the fatigue crack growth analyses were performed in two stages. First the crack was grown from a depth of 0.1 mm to 3 mm in steps of 0.1 mm using the sub-submodel shown in figure 8 (right). Next the crack geometry was imported into the submodel shown in figure 7 and grown further from a depth of 3 mm to the final crack depth of 29 mm in steps of 1 mm. The crack size at which the transition was made from the sub-submodel to the submodel was based on the minimum required mesh density in the submodel with respect to the crack size. To quantify the effect of the crack aspect ratio $a{:}\,c$, three different ratios ($1{:}\,2$, $1{:}\,3$ and $1{:}\,4$) were used that cover the most commonly used aspect ratios for fatigue analyses.

Load spectrum

The exact weight of the lifted coil, the position of the crane and the position of the trolley could be determined from SCADA data of one of the cranes operating in the hall where the girder is located. Data recorded over a period of seven months was processed to determine a representative load spectrum. Figure 9 shows the representative load spectrum and figure 10 the corresponding rainflow counted spectrum that is used as an input for both the hot spot stress based and fracture mechanics

based fatigue life analyses. For the fatigue life calculations it is assumed that this reference spectrum is repeated indefinitely until failure occurs. The finite element model is loaded with a unit load, the stress and stress intensity factors are scaled using the fatigue spectrum.

RESULTS AND DISCUSSION

The results of the fatigue lifetime calculations are shown in table 2. The number of cycles reported for the LEFM based lifetime calculation correspond to a crack growing from an initial size of 0.1 mm to a through-thickness crack of 29 mm depth. The crack growth simulations took approximately 38 hours to complete, the hot spot stress approach based on Miner's rule took less than 2 minutes. Both were performed on a workstation with 256 GB RAM using 4 cores running at 2.10 GHz.

A significant fatigue lifetime difference is observed between the endurance based and fracture mechanics based methods. Fatigue lifetimes determined using the LEFM based method are much shorter than the ones based on the HSS approach. For the HSS approach a lot of the cycle reversals fall below the knee-point stress range of the S-N curve, therefore they barely contribute to the damage tally. This effect is less pronounced for the LEFM based method as the propagation rate for all cycles is obtained from a single Paris law slope. As stated higher, an important difference is that the HSS approach, which is based on S-N curves, inherently includes both initiation and propagation number of cycles, whereas the LEFM based method only accounts for the propagation part. In some studies the parameters such as initial crack size and crack aspect ratio have been calibrated such that the probability of failure based on the fracture mechanics approach corresponds to that of S-N data [33]. In these cases the initial crack size was generally found to be extremely small (down to 0.005 mm as reported higher). However, LEFM based fatigue crack propagation calculations are known to lose validity for such shallow cracks (Miller [36]). Furthermore cracks of such sizes are impossible to detect in real structures of the scale considered in this paper.

To assess the sensitivity of the fracture mechanics based lifetime estimation to the material properties, an additional simulation was performed with the BS7910:2019 fatigue crack growth law applicable for $R < 0.5$ where $m = 8.16$ and $C = 7.64 \cdot 10^{-14}$. An increase in number of cycles with, approximately, a factor seven was found for the second stage of the simulation (3 mm depth to 29 mm). This difference of almost an order of magnitude, indicates that the results of the LEFM based method are very sensitive to the material parameters. In the scope of lifetime extension it is therefore crucial that accurate material data is available in order to obtain reliable results.

TABLE 2: Fatigue lifetime results for the hot spot stress approach (HSS) and the linear-elastic fracture mechanics (LEFM) approach for different initial aspect ratios ($a_0 = 0.1\ mm, a_f = 29\ mm$).

	HSS	LEFM		
		$a{:}c\ =\ 1/2$	$a{:}c\ =\ 1/3$	$a{:}c\ =\ 1/4$
Lifetime (cycles)	125 741 040	5 792 985	5 267 923	5 039 089

Table 3 shows the fatigue lifetime for three of the most common recommended final crack depths, namely $1/2\ t$, $1/3\ t$ and t, with t the plate thickness. Figure 11 shows the crack depth as a function

of the number of applied cycles starting from the initial crack depth of 0.1 mm to the final crack depth of 29 mm. The slope of the curve is initially small but rapidly increases as the crack depth becomes substantial with respect to the plate thickness. The results reveal that the choice of the final crack depth is less important in determining the total number of cycles than the choice of the initial crack depth. For the three LEFM simulations, a fatigue lifetime difference of approximately 10% is found between $a_f = 1/2\ t$ and $a_f = t$. Regardless of the initial aspect ratio, the crack growth from 0.1 mm to 3 mm accounts for approximately 70% of the obtained fatigue life.

TABLE 3: Linear-elastic fracture mechanics based fatigue lifetime for different aspect ratios and different final crack depth recommendations.

	$a:c\ =\ 1/2$	$a:c\ =\ 1/3$	$a:c\ =\ 1/4$
$a_f = t$	5 792 985	5 267 923	5 039 089
$a_f = \frac{2}{3}t$	5 517 892	4 980 486	4 756 158
$a_f = \frac{1}{2}t$	5 226 914	4 740 278	4 501 722

*t = 29 mm

As mentioned previously, the aspect ratio of the crack was not kept constant during the propagation stage as is often assumed in literature. The results obtained in this study show that a constant aspect ratio would not have been a valid assumption. First, it is clear from table 3 that the aspect ratio has a significant influence on the predicted fatigue life. A smaller aspect ratio and identical crack depth results in larger stress intensity factors along the crack front. Figure 12 shows the evolution of the aspect ratio as a function of the number of applied cycles. The three cracks grow towards approximately the same aspect ratio $a:c\ = 0.84$ and then continue growing at approximately the same rate in both depth and width directions. Since smaller aspect ratios result in larger stress intensity factors along the crack front (for the same crack depth) and the cracks evolve towards larger aspect ratios, a constant aspect ratio would thus be overly conservative. The transition between the sub-submodel and submodel are clearly visible in figure 12. The aspect ratios first reach an equilibrium in the small scale model and vary again after transitioning to the submodel. This is likely caused by the change in meshing size and difference between the stiffness of the submodels. A convergence study regarding an optimal mesh size and crack transition size between the two models is outside the scope of this work but should be the subject of a future work.

Figure 13 shows the crack growth stages and the evolution of the cracks for the complete fatigue crack growth simulations. The figure shows that all three cracks grew slightly asymmetrical. Crack growth rates were found to be larger at the side of the lattice support structure. The support structure is connected to the bottom flange of the main girders with gusset plates that are bolted to the bottom flange. The result is that the bottom flange is slightly stiffer at the side of the support structure which means that the stresses are higher at that side. The asymmetrical growth of the crack would not be taken into account if a 2D crack analysis is used, such as in [34]. Similarly, assuming a constant

crack aspect ratio would mean that the increased crack growth rate occurring in a different plane than the initial deepest point would not be accounted for.

CONCLUSIONS

A literature review revealed that there is only a limited amount of research on fatigue assessment of overhead crane runway girders. Moreover, the majority of literature is devoted to fatigue assessment using the nominal stress approach. Literature on the application of more advanced assessment methods such as the hot spot stress and fracture mechanics based approaches is severely lacking.

A finite element model of an in-service overhead crane runway girder was developed and validated using optical fibre strain measurements. Based on the results of the finite element model and on-site experience with similar girders, a fatigue critical detail was selected for a fatigue assessment study. The IIW based hot spot stress endurance approach and fracture mechanics based assessments were compared. The hot spot stress based fatigue lives were determined using an in-house developed framework. For the fatigue crack growth simulations, a new framework was developed that uses XFEM-based stress intensity factor solutions to determine how the crack propagates and the corresponding fatigue life.

Using SCADA data from one of the crane on operating on the studied girder, a representative reference load spectrum was obtained. This reference spectrum was used as in input of both the hot spot stress and the fracture mechanics based approaches. Fatigue crack growth simulations were performed for three different initial aspect ratio's.

A difference in fatigue lifetime estimation of almost two orders of magnitude was observed between the results of HSS and LEFM based methods. For the fracture mechanics approach it was found that the results are very sensitive to both the initial crack dimensions and the fatigue crack propagation material properties. On the other hand, the effect of the final crack length was found to relatively insignificant. It was also observed that the three studied cracks evolve towards a similar crack aspect ratio and then continue growing with approximately the same rate in the depth and width directions. Furthermore, the cracks exhibited asymmetrical crack growth due to asymmetry in the global stiffness of the crane girder, which influences the crack growth rates along the crack front. A smaller crack aspect ratio a:c and identical crack depth result in larger stress intensity factors along the crack front. The use of either 2D crack propagation simulations or 3D crack growth propagation simulations with a constant crack aspect ratio would therefore lead to unsatisfactory results for complex joints.

ACKNOWLEDGEMENTS

The authors acknowledge the financial support of Vlaio through the SafeLife project (project number 179P04718W) and also the support of SIM (Strategic Initiative Materials in Flanders) and IBN Offshore Energy.

[1] T. Tominaga, K. Matsuoka, Y. Sato, and T. Suzuki, “Fatigue improvement of weld repaired crane runway girder by ultrasonic impact treatment,” *Welding in the World*, vol. 52, no. 11/12, 2008.

[2] R. S. Milman, “Fatigue Life Analyses of Crane Runway Girders,” *Iron and Steel engineer*, vol. 73, no. 7, pp. 44–48, 1996, [Online]. Available: https://www.tib.eu/en/search/id/BLSE%3ARN010593554/Fatigue-life-analyses-of-crane-runway-girders/.

[3] A. B. Patrikeev, “Certain laws of fatigue damages in welded crane girders,” *Strength of Materials*, vol. 15, no. 7, p. 906, 1982, doi: https://doi.org/10.1007/BF01528930.

[4] H. Kuwamura and M. Hanzawa, “Inspection and repair of fatigue crack in crane runway girders,” *Journal of structural engineering*, vol. 113, no. 11, pp. 2181–2194, 1987.

[5] D. A. Demo and J. W. Fisher, “Analysis of fatigue of welded crane runway girders,” *Journal of the Structural Division*, vol. 102, no. 12106 Proc Paper, 1976.

[6] J. Wardenier, P. de Vries, and G. Timmermann, “Evaluation of cracks in an offshore crane runway girder,” *Steel Construction*, vol. 10, no. 1, pp. 67–71, Jan. 2017, doi: 10.1002/stco.201710011.

[7] G. Ávila, E. Palma, and R. de Paula, “Crane girder fatigue life determination using SN and LEFM methods,” *Engineering Failure Analysis*, vol. 79, no. May, pp. 812–819, 2017, doi: 10.1016/j.engfailanal.2017.05.027.

[8] O. Caglayan, K. Ozakgul, O. Tezer, and E. Uzgider, “Fatigue life prediction of existing crane runway girders,” *Journal of Constructional Steel Research*, vol. 66, no. 10, pp. 1164–1173, 2010, doi: 10.1016/j.jcsr.2010.04.009.

[9] AASHTO, “Standard Specifications For Highway Bridges,” DC, Washington, 1996.

[10] X. Tong, Y. C. Tuan, J. Yang, J. Zhang, and Q. Yue, “Fatigue Strength of End-Coped Crane Runway Girders,” *Journal of structural engineering*, vol. 133, no. 12, pp. 1783–1791, 2007, doi: 10.1061/ASCE0733-94452007133:121783.

[11] F. Pelayo, C. Rodríguez, and A. F. Canteli, “Failure and repair analysis of a runway beam: Influence of the standard applied to lifetime prediction,” *Engineering Failure Analysis*, vol. 56, pp. 89–97, Oct. 2015, doi: 10.1016/j.engfailanal.2015.04.008.

[12] J. Wardenier, P. de Vries, and G. Timmerman, “Fatigue behaviour of a welded I-section under a line load in compression,” *Journal of Constructional Steel Research*, vol. 128, pp. 210–218, 2017, doi: 10.1016/j.jcsr.2016.08.022.

[13] P. Kossakowski, W. Wciślik, and M. Bakalarz, “Failure of the overhead crane runway,” Jul. 2019, doi: 10.1051/matecconf/201928.

[14] S. Citarelli and M. Feldmann, “Fatigue Failure of runway beams due to wheel loads,” in *14th Nordic Steel Construction Conference*, Sep. 2019, vol. 3, no. 3–4, pp. 621–628, doi: 10.1002/cepa.1110.

[15] V. Vašková, R. Fojtík, and D. Pustka, “Analysis of a Crane Runway Failure,” in *Procedia Engineering*, 2017, vol. 190, pp. 255–262, doi: 10.1016/j.proeng.2017.05.335.

[16] A. Hobbacher, *Recommendations for fatigue design of welded joints and components*, 2nd edition., no. IIW-2259-15. Springer, 2016.

[17] E. Niemi, W. Fricke, and S. J. Maddox, *Structural Hot-Spot Stress Approach to Fatigue Analysis of Welded Components*, 2nd ed. Springer, 2018.

[18] F. Z. Akhlaghi, “Fatigue life assessment of welded bridge details using structural hot spot stress method,” 2009.

[19] T. H. T. Chan, T. Q. Zhou, Z. X. Li, and L. Guo, “Hot spot stress approach for Tsing Ma Bridge fatigue evaluation under traffic using finite element method,” *Structural Engineering and Mechanics*, vol. 19, no. 3, pp. 261–279, 2005, doi: 10.12989/sem.2005.19.3.261.

[20] Y. Ding, Y. Song, D. Ph, B. Cao, G. Wang, and A. Li, “Full-Range S-N Fatigue-Life Evaluation Method for Welded Bridge Structures Considering Hot-Spot and Welding Residual Stress,” *Journal of Bridge Engineering*, vol. 21, no. 12, pp. 1–10, 2016, doi: 10.3892/ol.2014.2462.

[21] K. Hectors and W. de Waele, “Modeling nonlinear fatigue damage accumulation in a welded runway girder,” *Procedia Structural Integrity*, vol. 28, pp. 239–252, 2020, doi: https://doi.org/10.1016/j.prostr.2020.10.030.

[22] P. Rettenmeier, E. Roos, and S. Weihe, “Fatigue analysis of multiaxially loaded crane runway structures including welding residual stress effects,” in *International Journal of Fatigue*, Jan. 2016, vol. 82, pp. 179–187, doi: 10.1016/j.ijfatigue.2015.04.009.

[23] P. Rettenmeier, E. Roos, S. Weihe, and X. Schuler, “Assessment of mixed mode crack propagation of crane runway girders subjected to cyclic loading,” *ENGINEERING FRACTURE MECHANICS*, vol. 153, pp. 11–24, 2016, doi: 10.1016/j.engfracmech.2015.12.018.

[24] K. Hectors, H. de Backer, M. Loccufier, and W. de Waele, “Numerical framework for fatigue lifetime prediction of complex welded structures,” *Frattura ed Integrita Strutturale*, vol. 14, no. 51, pp. 552–566, Jan. 2020, doi: 10.3221/IGF-ESIS.51.42.

[25] BSI, “BS 7910:2019 Guide to methods for assessing the acceptability of flaws in metallic structures,” 2019.

[26] D. Radaj, C. M. Sonsino, and W. Fricke, “Crack propagation approach for seam-welded joints,” *Fatigue Assessment of Welded Joints by Local Approaches*, pp. 233–295, 2006, doi: 10.1533/9781845691882.233.

[27] D. Radenkovic, “Stress analysis in tubular joints,” *Steel in Marine Structures, Special and Plenary Sessions*, pp. 53–95, 1981.

[28] T. Bokalrud and A. Karlsen, “Probabilistic fracture mechanics evaluation of fatigue failure from weld defects in butt welded joints.,” 1982.

[29] E. Ayala-Uraga and T. Moan, “Fatigue reliability-based assessment of welded joints applying consistent fracture mechanics formulations,” *International Journal of Fatigue*, vol. 29, no. 3, pp. 444–456, Mar. 2007, doi: 10.1016/j.ijfatigue.2006.05.010.

[30] T. Moan, N.-C. Hellevig, K. Skjoldli, and Ole T. Vardal, “Torgeir Moan Initial Crack Depth and POD Values Inferred From In-Service Observations of Cracks in North Sea Jackets,” *Journal of Offshore Mechanics and Arctic Engineering*, vol. 122, no. 3, pp. 157–162, 2000, doi: https://doi.org/10.1115/1.1286676.

[31] T. R. Gurney, *Fatigue of welded structures*. CUP Archive, 1979.

[32] A. Schumacher, L. C. Borges, and A. Nussbaumer, “A critical examination of the size effect correction for welded steel tubular joints,” *International Journal of Fatigue*, vol. 31, no. 8–9, pp. 1422–1433, Aug. 2009, doi: 10.1016/j.ijfatigue.2009.04.003.

[33] I. Lotsberg, “Assessment of the size effect for use in design standards for fatigue analysis,” *International Journal of Fatigue*, vol. 66, pp. 86–100, 2014, doi: 10.1016/j.ijfatigue.2014.03.012.

[34] K. Rykaluk, K. Marcinczak, and S. Rowiński, “Fatigue hazards in welded plate crane runway girders – Locations, causes and calculations,” *Archives of Civil and Mechanical Engineering*, vol. 18, no. 1, pp. 69–82, 2018, doi: 10.1016/j.acme.2017.05.003.

[35] J. Qian and A. Fatemit, “Mixed mode fatigue crack growth: A literature survey,” 1996.

[36] K. I. Miller, “The Short Crack Problem,” *Fatigue and Fracture of Engineering Materials and Structures*, vol. 5, no. 3, pp. 223–232, Jul. 1982.

FIGURE 1: Principal components of an overhead crane assembly.

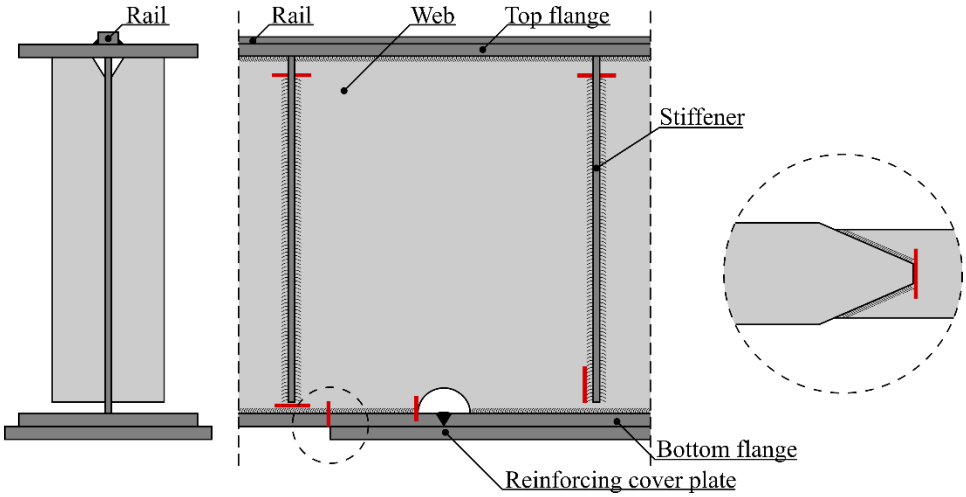

FIGURE 2: Typical crack locations (in red) in a welded crane runway girder, based on [34].

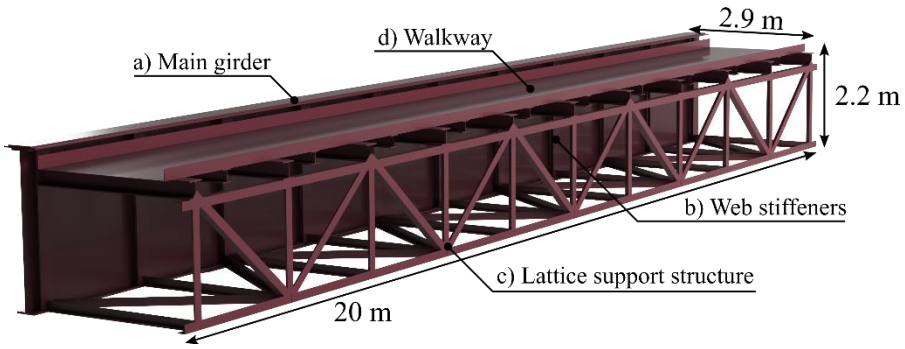

FIGURE 3: Global model of the studied crane girder

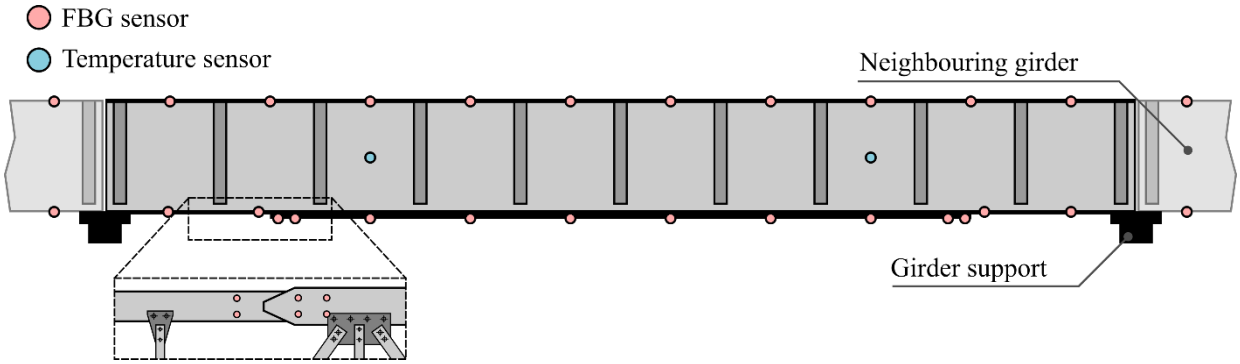

FIGURE 4: Location of the sensor points on the overhead crane girder.

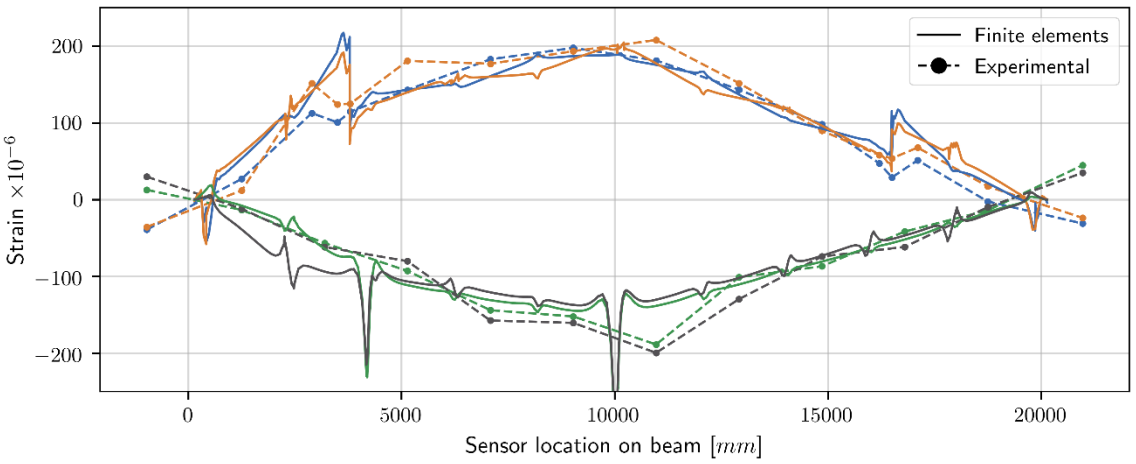

FIGURE 5: Optical fiber strain measurements of the studied girder compared to strains extracted from the finite element model for the same loading condition. Strains measured at the top flange (compression) and at the bottom flange (tension) are shown. Each color corresponds to a single sensor line.

FIGURE 6: Fatigue cracks observed at cover plate ends in the bottom flange of crane girders

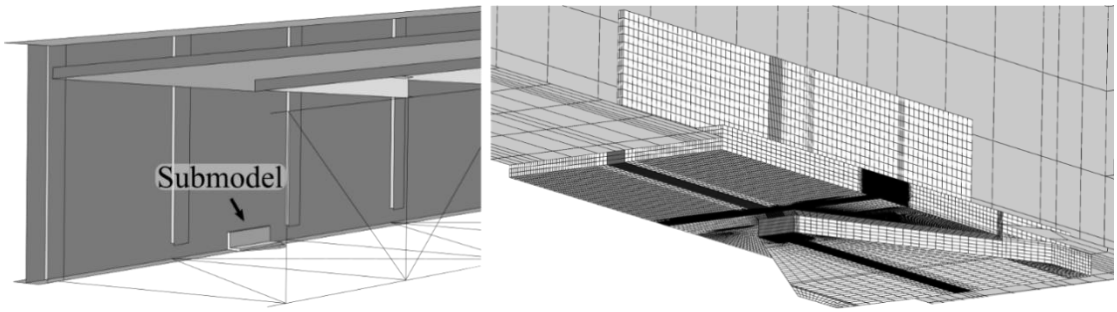

FIGURE 7: Overlay plot of the submodel in the global model, illustrating the modelling space transition (shell to solid) and the increased mesh density of the submodel compared to the global model.

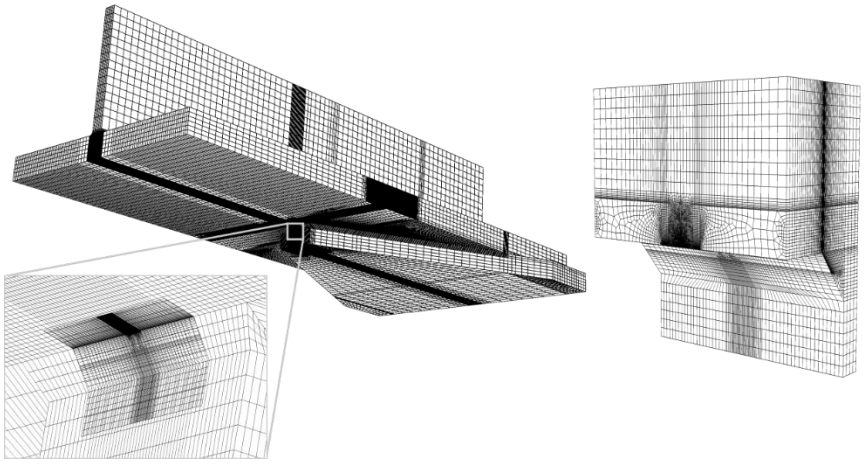

FIGURE 8: Overlay of the sub-submodel and the submodel (left). The isolated sub-submodel (right).

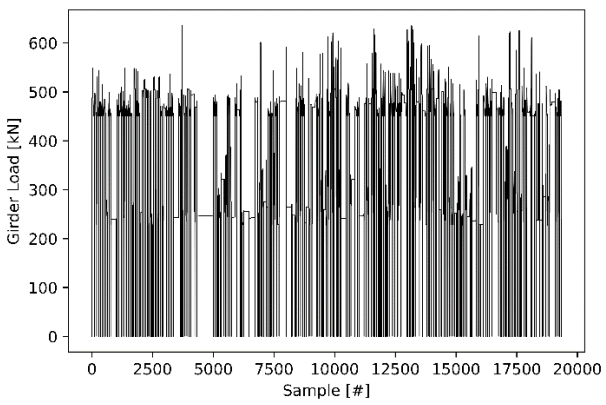

FIGURE 9: Load spectrum crane girder

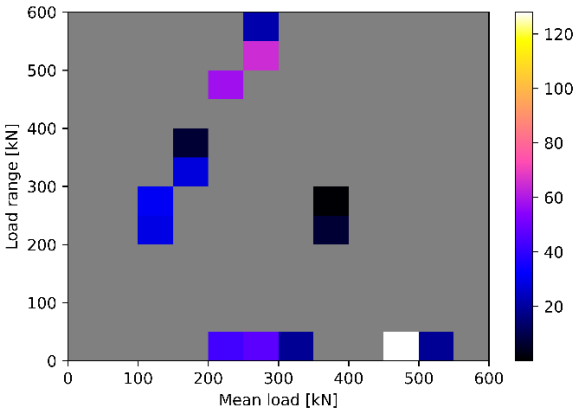

FIGURE 10: Rainflow counted load spectrum, the colors correspond to the number of cycles in each load bin.

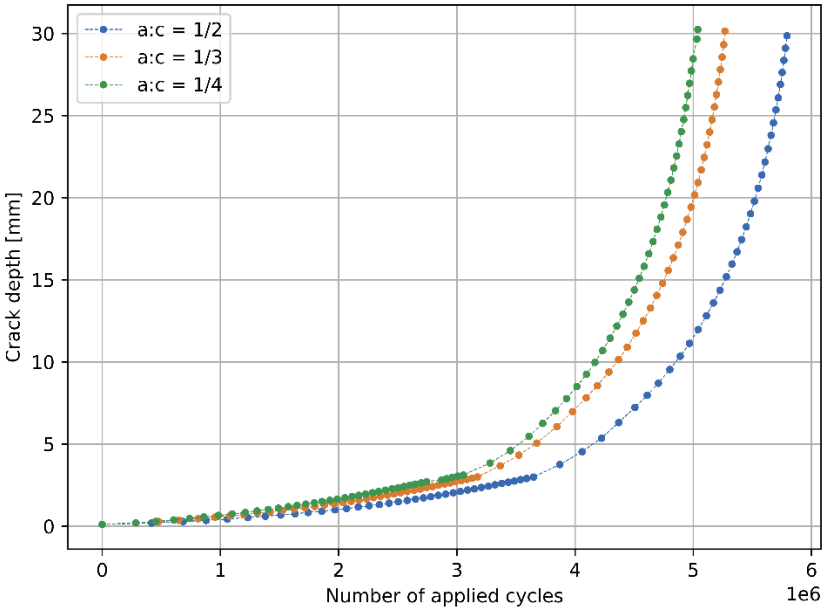

FIGURE 11: Evolution of crack depth as a function of the number of applied cycles obtained from the simulations using the sub-submodel and submodel of the studied crane girder detail.

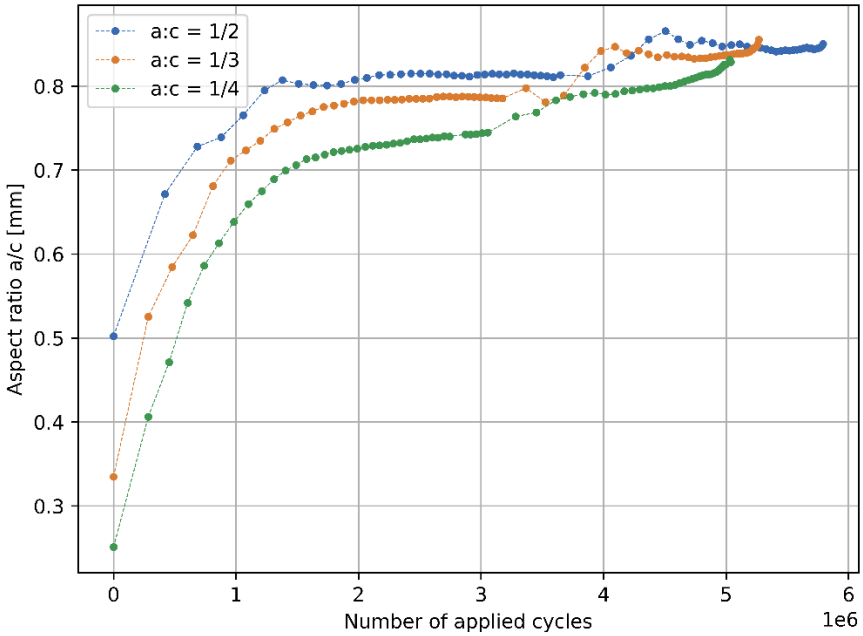

FIGURE 12: Evolution of the aspect ratio as a function of the number of applied cycles obtained from the crack growth simulations in the small and large scale submodels of the studied crane girder detail.

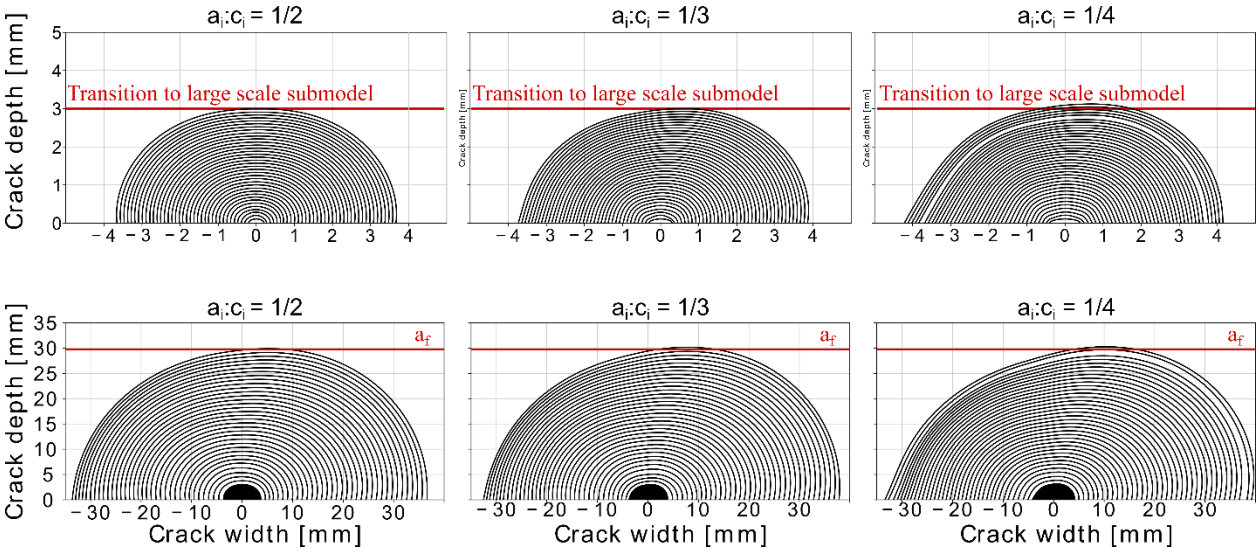

FIGURE 13: Final crack shape and crack growth steps obtained from the crack growth simulations in the sub-submodel (top) and submodel (bottom) of the studied crane girder detail. The final crack length for both propagation calculations is indicated.